Electronic Supplementary Information

# Ultrathin $MoS_2$ nanosheets homogenously embedded in N, O co-doped carbon matrix for high-performance lithium and sodium storage

Meisheng Han, Zijia Lin, and Jie Yu*

Shenzhen Engineering Lab for Supercapacitor Materials, Shenzhen Key Laboratory for Advanced Materials, Department of Material Science and Engineering, Harbin Institute of Technology, Shenzhen, University Town, Shenzhen 518055, China
*E-mail: jyu@hit.edu.cn

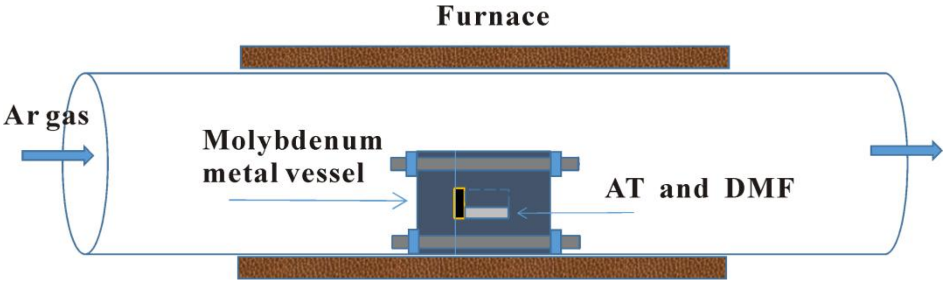


**Fig. S1** Schematic diagram of synthesizing apparatus

The vessel consists of molybdenum vessel, copper ring, and molybdenum screw. The molybdenum vessel consists of two parts, namely upper lid and lower container with a volume of 5 ml. The copper ring plays a role of sealing. The molybdenum screws are for connecting and fastening of the lid and container.

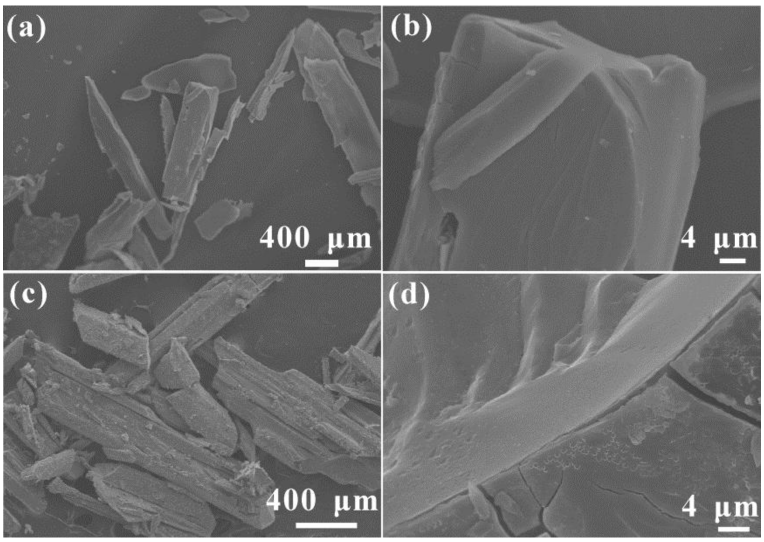


**Fig. S2** SEM images of pure $MoS_2$ (a,b) and AT (c,d).

**Table S1** Fitting results of XPS spectra of all the samples.

| Samples | Mo (at%) | S (at%) | C (at%) | N (at%) | O (at%) |
|---|---|---|---|---|---|
| $MoS_2$ | 29.18 | 57.66 | 10.04 | — | 3.12 |
| $MoS_2$/C -I | 2.12 | 4.09 | 72.19 | 13.41 | 8.19 |
| $MoS_2$/C -II | 3.08 | 5.99 | 71.43 | 12.81 | 6.69 |
| $MoS_2$/C-III | 3.63 | 7.08 | 70.56 | 12.20 | 6.53 |

The atomic ratio of S and Mo elements in the $MoS_2$, $MoS_2$/C–I, $MoS_2$/C–II and $MoS_2$/C-III is 1.98, 1.93, 1.94 and 1.95, respectively. The doping amount of N and O elements in the carbon materials should be calculated by N (at%)/(C (at%)+N (at%)+O (at%))*100% and O (at%)/(C (at%)+N (at%)+O (at%))*100%, respectively. Therefore, the doping amount of N and O elements in the carbon materials of $MoS_2$/C–I is 14.30 at% and 8.73 at%, respectively. The doping amount of N and O elements in the carbon materials of $MoS_2$/C–II is 14.09 at% and 7.36 at%, respectively. The doping amount of N and O elements in the carbon materials of $MoS_2$/C–III is 13.67 at% and 7.31 at%, respectively.

**Table S2** The elemental analysis results of the obtained samples.

| Samples | C (wt%) | N (wt%) | O (wt%) | $MoS_2$ (wt%) |
|---|---|---|---|---|
| $MoS_2$/C-I | 31.3 | 5.6 | 3.3 | 59.8 |
| $MoS_2$/C-II | 19.1 | 3.5 | 1.7 | 75.7 |
| $MoS_2$/C-III | 10.2 | 1.5 | 0.8 | 87.5 |

**Table S3** The charge capacity (mAh $g^{-1}$) and charge capacity retention (%) after 100 cycles of the obtained samples.

| Samples | First capacity | Final capacity | Capacity retention |
|---|---|---|---|
| $MoS_2$ | 663.1 | 260.3 | 39.3 |
| $MoS_2$/C-I | 812.3 | 815.8 | 100.4 |
| $MoS_2$/C-II | 909.3 | 946.3 | 104.1 |
| $MoS_2$/C-III | 768.7 | 649.9 | 84.6 |

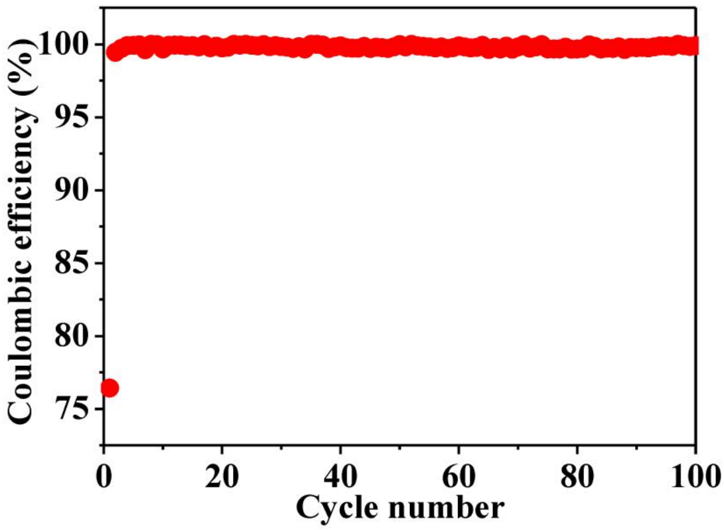


**Fig. S3** CE of $MoS_2$/C-II nanocomposite at 0.1 C during 100 cycles.

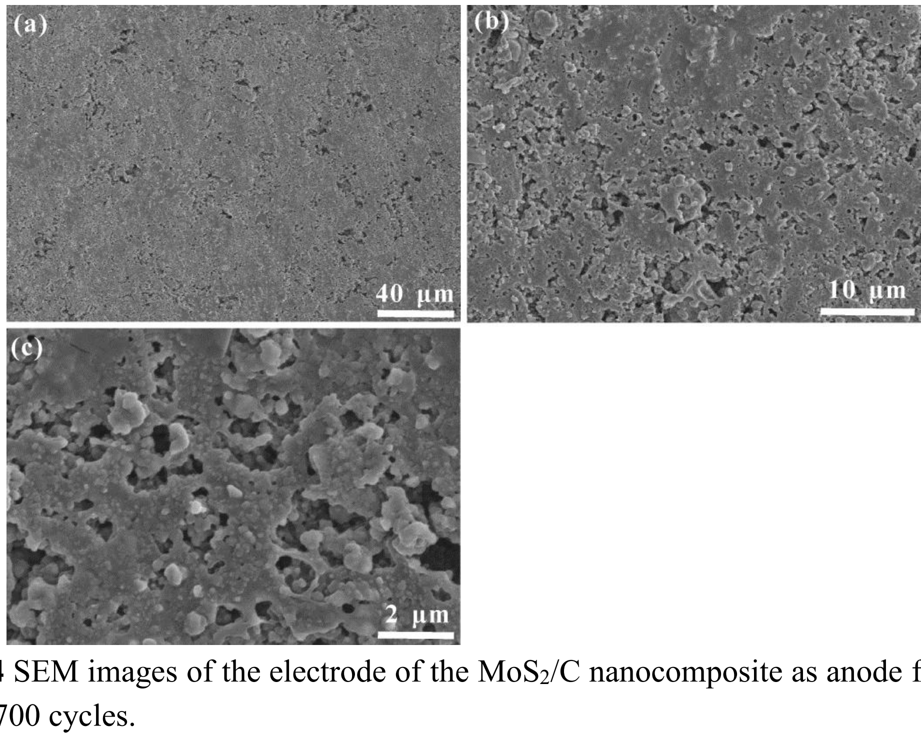


**Fig. S4** SEM images of the electrode of the $MoS_2$/C nanocomposite as anode for LIBs after 2700 cycles.

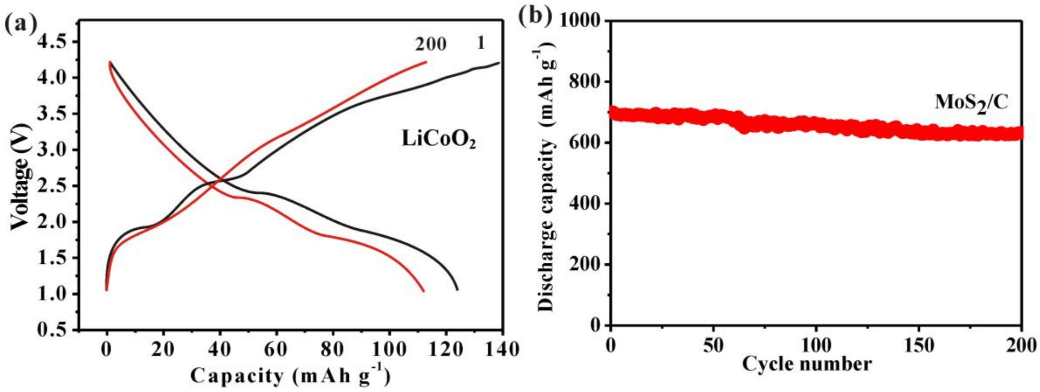


**Fig. S5** (a) Charge/discharge curves and (b) Cycling curve of $MoS_2$/C/$LiCoO_2$ full cell at 1 C.

**Table S4** Performance comparison of full cells at high current density. Commercial graphite anode, $LiCoO_2$ cathode, $LiFePO_4$ cathode, polyvinylidene fluoride binder, and acetylene black conductive additive were used to assemble the full cells. $A_{DC}$-anode discharge capacity (mAh g$^{-1}$), $C_{DC}$-cathode discharge capacity (mAh g$^{-1}$), $C_R$-capacity retention (%), J-current density (C), $N_C$-cycle number, NA-not available.

| Anode/cathode | $A_{DC}$ | $C_{DC}$ | $C_R$ | J | $N_C$ | References |
|---|---|---|---|---|---|---|
| $MoS_2$/C/$LiCoO_2$ | 632.8 | 112.7 | 90.4 | 1 | 200 | This work |
| Graphite/$LiCoO_2$ | NA | 26.0 | 21.0 | 1 | 200 | *Adv. Energy Mater.*, 2013, **3**, 213–219 |
| Graphite/$LiCoO_2$ | 274.0 | NA | 85.6 | 0.5 | 100 | *J. Power Sources,* 2010, **195**, 2368–2371 |
| Graphite/$LiFePO_4$ | 224.0 | 98.0 | 70.0 | 1 | 200 | *J. Power Sources*, 2011, **196**, 7707–7714 |

**Table S5** Electrochemical performances of $MoS_2$-based materials for LIB anodes in open reports. $C_C$-charge capacity (mAh $g^{-1}$), $C_R$-capacity retention (%), $M_L$-mass loading (mg $cm^{-2}$), J-current density (A $g^{-1}$), $N_C$-cycle number, NA-not available.

| Samples | $C_C$ | $C_R$ | $M_L$ | J | $N_C$ | References |
|---|---|---|---|---|---|---|
| $MoS_2$/C | 946.2 | 104.3 | 1.20 | 0.067 | 100 | This work |
| $MoS_2$/C | 702.3 | 115.4 | 1.20 | 1.34 | 2700 | This work |
| $MoS_2$/C | 234.7 | NA | 1.20 | 13.4 | NA | This work |
| $MoS_2$/ $Mo_2TiC_2T_x$ | 509 | 91.88 | NA | 0.1 | 100 | *Angew. Chem. Int. Ed.*, 2018**,** **57**, 1846-1850. |
| $MoS_2$/ $Mo_2TiC_2T_x$ | 182 | NA | NA | 2 | NA | *Angew. Chem. Int. Ed.*, 2018**,** **57**, 1846-1850. |
| CNT@$MoS_2$@C | 905 | NA | 1.00 | 1 | 500 | *Adv. Energy Mater.*, 2018**, 8**, 1700174. |
| RGO/$MoS_2$ | 892 | 93.89 | 0.41 | 2 | 400 | *Energy Storage Mater.*, 2018**, 10**, 282-290. |
| RGO/$MoS_2$ | 723 | NA | 0.41 | 10 | NA | *Energy Storage Mater.*, 2018**, 10**, 282-290. |
| Graphene@$MoS_2$ nanotubes | 830 | 96.5 | 1.10 | 0.4 | 120 | *Energy Storage Mater.*, 2017**, 9**, 188-194. |
| Graphene@$MoS_2$ nanotubes | 502 | NA | 1.10 | 2 | NA | *Energy Storage Mater.*, 2017**, 9**, 188-194. |
| $MoS_2$@C | 993 | NA | NA | 1 | 200 | *ACS Nano*, 2017**, 11**, 8429-8436. |
| $MoS_2$@C | 595 | NA | NA | 10 | NA | *ACS Nano*, 2017**, 11**, 8429-8436. |
| TNO@MSHRs | 740 | 91.58 | 1.10 | 1 | 200 | *ACS Nano*, 2017**, 11**, 1026-1033. |
| TNO@MSHRs | 611 | NA | 1.10 | 4 | NA | *ACS Nano*, 2017**, 11**, 1026-1033. |
| Carbon@$MoS_2$ | 740 | NA | NA | 0.1 | 100 | *Adv. Mater.*, 2016**, 28**, 10175-10181. |
| $MoS_2$ nanospheres | 1100 | 86.61 | NA | 0.5 | 100 | *Angew. Chem. Int. Ed.*, 2016**, 128**, 7549-7552. |
| NG-$MoS_2$ | 980 | NA | 2.00 | 1 | 400 | *ACS Nano*, 2016**, 10**, 8526-8535. |
| C@$MoS_2$ nanoboxes | 1000 | NA | 1.00 | 0.4 | 200 | *Angew. Chem. Int. Ed.*, 2016**, 55**, 12783-12788 |
| $MoS_2$/G | 907 | 83.98 | NA | 1 | 400 | *Angew. Chem. Int. Ed.*, 2015**,** **54**, 7395-7398. |

| | | | | | | |
|---|---|---|---|---|---|---|
| $MoS_2$ nanospheres | 1009.2 | 80.74 | 1.00 | 0.5 | 500 | *ACS Nano*, 2015, **9**, 12464-12472. |
| 3DFL-$MoS_2$@PCNNs | 709 | 95.2 | NA | 2 | 520 | *ACS Nano*, 2015, **9**, 3837-3848. |
| NTL-$MoS_2$/G | 1033 | 91.66 | NA | 0.1 | 220 | *Nano Energy*, 2014, **10**, 144-152. |
| $MoS_2$/GS films | 907 | NA | NA | 1 | 1000 | *Nano Energy*, 2014, **8**, 183-195. |

**Table S6** Electrochemical performances of $MoS_2$-based materials for SIB anodes in open reports. $C_C$-charge capacity (mAh $g^{-1}$), $C_R$-capacity retention (%), $M_L$-mass loading (mg $cm^{-2}$), J-current density (A $g^{-1}$), $N_C$-cycle number, NA-not available.

| Samples | $C_C$ | $C_R$ | $M_L$ | J | $N_C$ | References |
|---|---|---|---|---|---|---|
| $MoS_2$/C | 419.5 | 91.5 | 1.20 | 0.067 | 100 | This work |
| $MoS_2$/C | 187.9 | NA | 1.20 | 3.35 | NA | This work |
| M-c $MoS_2$ | 401 | 89.1 | NA | 0.2 | 150 | *Nano Energy*, 2018, **51**, 546. |
| RGO/$MoS_2$ | 312 | 71.3 | 0.41 | 1 | 600 | *ACS Nano*, 2017, **11**, 8429. |
| $MoS_2$/graphene | 313 | 71.95 | NA | 0.05 | 200 | *Adv. Funct. Mater.*, 2017, **27**, 1702998. |
| $MoS_2$@C-CMC | 286 | 80.56 | NA | 0.08 | 100 | *Adv. Energy Mater.*, 2016, **6**, 1502161. |
| $MoS_2$ nanosheet | 330 | 33.67 | 1.20 | 0.08 | 100 | *Adv. Energy Mater.*, 2015, **5**, 1401205. |

**Table S7** Rate capability of different kinds of materials for LIB anode in open reports. $C_C$-charge capacity (mAh $g^{-1}$), J-current density (C or A $g^{-1}$). 1 C indicates the current density when the anodes are charged to the theoretical capacity in one hour.

| Samples | $C_C$ | J | References |
|---|---|---|---|
| $MoS_2$/C | 234.7 | 20 C | This work |
| Sn hybrid composite | 150 | 20 C | *Nano Lett.*, 2018, **18**, 467-474. |
| $Nb_{18}W_{16}O_{93}$ | 70 | 100 C | *Nature*, 2018, **559**, 556-563. |
| Si-nanolayer-embedded graphite/carbon hybrids | 222.3 | 5 C | *Nat. Energy*, 2016, **1**, 16113. |
| $SiO_x$/$SiO_y$ nanomembrane | 4 | 10 A $g^{-1}$ | *Adv. Mater.*, 2014, **26**, 4527-4532. |
| $SnO_2$NC@N-RGO | 417 | 20 A $g^{-1}$ | *Adv. Mater.*, 2013, **25**, 2152-2157. |
| Si nanotube | 540 | 20 C | *Nat. Nanotechnol.*, 2012, **7**, 310-315. |
| $Li_4Ti_5O_{12}$ nanowire | 119.4 | 30 C | *Adv. Mater.*, 2012, **24**, 6502-6506. |

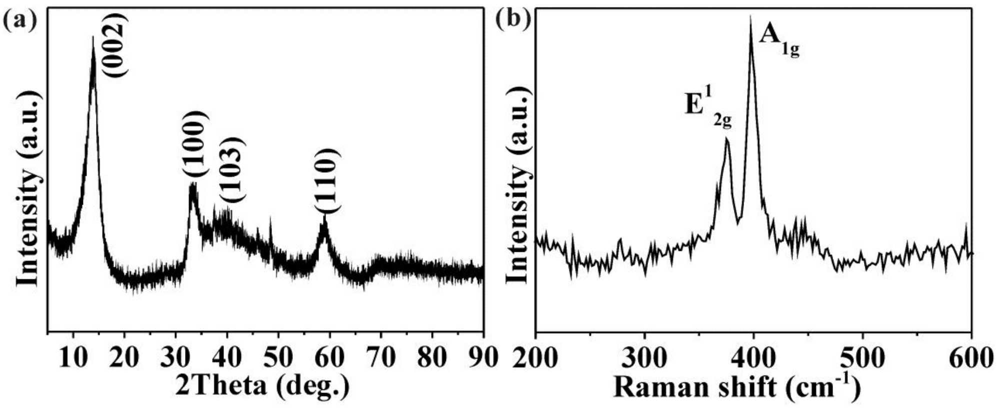


**Fig. S6** (a) XRD pattern and (b) Raman spectrum of sample obtained by heating pure AT at 360 °C in the sealed vessel.

From XRD pattern, the sample shows the peaks of (002), (110), (103) and (110) crystal plane of 2H-$MoS_2$. From the Raman spectrum, the sample shows the peaks of the $E^1_{2g}$ (in-plane vibration) and $A_{1g}$ (out of plane vibration) modes of 2H-$MoS_2$. The above results indicate $MoS_2$ has been obtained at 360 °C, namely AT can be fully changed into $MoS_2$ at 360 °C.

**Description of safety issues in the preparation process of samples**

It is necessary to discuss the safety issues during sample preparation using the sealed vessels as high pressure is generated in the process. In order to avoid too high pressure we adhere to three rules. First, the vessel volume could not be too big. Second, the amount of the reagents loaded could not be too large. Third, the flammable reagents could not be used. In this work, the vessel volume is 5 ml and the reagent amount loaded is 1.5 g. The reagents of AT and DMF is not flammable, which decompose and react gradually when heating. Presently, we have no tools to measure the pressure in the vessel. But we could estimate the pressure roughly using the ideal gas equation (PV=nRT). As an example, we calculated the pressure when loading the mixture of 0.5 g AT and 1 g DMF. According to idea gas state equation, when T is 426 K (the boiling point of DMF), the pressure is calculated to be 9.1 MPa if the DMF was totally evaporated. Above 633 K, DMF starts to gradually decompose into gaseous free radicals mainly OHCN:, OHC·and ·$CH_3$ etc. (*Carbon*, 2004, **42**, 2625-2633.) Therefore, the pressure at 633 K generated from DMF is 40.0 MPa. Subsequently, with further increasing temperature these gaseous free radicals start to convert into solid carbon and $H_2$. If only considering the pressure generated by $H_2$, the pressure will reach 137.9 MPa at 873 K. Simultaneously, the AT decomposes into $NH_3$ and $H_2S$ at 360 °C. For 0.5 g AT, the pressure generated by the $NH_3$ and $H_2S$ is 8.0 MPa at 633 K and 11.0 Mpa at 873 K. So the total pressure at 873 K is 148.9 MPa. We used 4 Mo screws with diameter of 6 mm. These 4 screws can support a force of $6.78\times10^4$ N at 293 K (*Nature Mater.*, 2013, **12**, 344-350). Based on the previous research on the influence of temperature on the tensile properties, the tensile strength would decrease about 37% from 293 K to 873 K. (*Acta Mater.,* 2013, **61**, 5743–5755). Therefore, the 4 screws can support a force of about $4.27\times10^4$ N at 873 K, which is higher than the force generated by the internal pressure in the vessel. If the pressure is too high, the screws will deform and elongate because Mo is plastic, resulting in the leakage of the gases. So for this reaction vessel the operation is safe. Up to now, we have not encountered safety problems. We believe that high productivity could be achieved by appropriately designing special instrument.